Tailoring of infrared photorefractive properties of Sn2P2S6 crystals by Te and Sb doping

Tobias Bach, Mojca Jazbinsek, G. Montemezzani, Peter Gunter, Alexander A. Grabar, Yulian Vysochanskii

Tailoring of infrared photorefractive properties of $Sn_2P_2S_6$ crystals by Te and Sb doping

Tobias Bach,[1,*] Mojca Jazbinšek,[1] Germano Montemezzani,[1] Peter Günter,[1] Alexander A. Grabar,[2] and Yulian M. Vysochanskii[2]

[1]*Nonlinear Optics Laboratory, ETH Zurich, CH-8093 Zurich, Switzerland*

[2]*Institute of Solid State Physics and Chemistry, Uzhgorod National University, 88 000 Uzhgorod, Ukraine*

[*]*Corresponding author: tbach@phys.ethz.ch*

The photorefractive properties of $Sn_2P_2S_6$ crystals doped with Te and Sb in the near-infrared wavelength range up to 1064 nm are reported. The main photorefractive parameters, i.e., two-wave mixing gain, effective electro-optic coefficient, diffusion length, concentration of traps, and response time, are compared with conventional nominally pure $Sn_2P_2S_6$. Te-doped $Sn_2P_2S_6$ shows the fastest response with the smallest decrease of the photorefractive efficiency with increasing wavelength in the near infrared. Sb doping, on the other hand, inhibits photorefraction in the near infrared. $Sn_2P_2S_6$:Te and $Sn_2P_2S_6$:Sb crystals both show a high two-wave mixing gain Γ at 633 nm, and 10 and 20 cm^{-1}. Te-doped $Sn_2P_2S_6$ shows a photorefractive gain of 4.5 cm^{-1} at 1064 nm. Response times at 1064 nm of 20 ms have been measured for the intensity 6 W/cm^2, which is 2 orders of magnitude shorter than in Rh-doped $BaTiO_3$.

1. INTRODUCTION

Photorefractive materials have been considered to be attractive candidates for several applications in photonics [1], particularly for the spatial and spectral laser beam clean-up using dynamic holography. However, conventional photorefractive crystals (mainly oxides) tend to show a reduced photorefractive sensitivity at larger wavelengths in the near infrared. Due to widely available powerful infrared laser sources, a substantial effort was made to improve the photorefractive sensitivity of these materials in this spectral range to use the photorefractive effect in devices. This can be achieved by the variation of the growth parameters (i.e., by changing the stoichiometry of the crystals), a reduction or oxidization treatment, and by doping of the photorefractive crystals. Examples of successfully improved photorefractive crystals for the near infrared are rhodium (Rh)-doped $BaTiO_3$ [2] and Rh-doped $KNbO_3$ [3]. $BaTiO_3$:Rh was successfully implemented for spatial beam clean-up by two-wave mixing energy transfer at 1.06 μm [4,5], as an external-cavity phase conjugating element for spatial and spectral clean-up of high-power laser diodes [6,7], and intracavity dynamic filter [8]. However, $BaTiO_3$:Rh suffers from domain formation caused by infrared light and has a phase transition close to room temperature at ~9 °C; therefore a new material is needed for these applications [9].

Tin thiohypodiphosphate ($Sn_2P_2S_6$) is a relatively new photorefractive material with a smaller bandgap (~2.3 eV) compared with conventional wide-bandgap oxide ferroelectrics [10]. The investigations of $Sn_2P_2S_6$ for photorefractive applications in the infrared were started by Odoulov *et al.* [11], where the photorefractive effect at a wavelength of 1064 nm with focused light and using preillumination with nominally pure (yellow) samples was demonstrated. Measurement of the electro-optical properties showed a high electro-optic coefficient of r_{111} = 160 pm/V at 1064 nm that corresponds to a half-wave voltage of V_π = 290 V, i.e., more than 1 order of magnitude smaller than the one measured in $LiNbO_3$ [12]. Nominally pure (yellow) $Sn_2P_2S_6$ crystals typically exhibit a great variation of parameters between different samples, and can be basically divided in two groups [10]. Crystals of type I show a pronounced electron-hole competition and a strong influence on preillumination and are of fundamental importance due to the unique electron-hole competing dynamics. Particularly, this allows to demonstrate a coherent optical oscillator with periodic zero-π phase modulation [13]. On the other hand, for crystals of type II no considerable transient gain and preillumination influence are detected, and these samples are preferable for applications requiring a high steady-state photorefractive gain. Self-pumped optical phase conjugation in these crystals was realized up to a wavelength of 1064 nm [14,15]. Besides, $Sn_2P_2S_6$ is interesting for fast interband photorefraction in the visible, i.e., excitation of the near-surface gratings by 514 nm wavelength, with a response of 100 μs at an intensity of 0.6 W/cm^2 [16]. In nonlinear optics, $Sn_2P_2S_6$ shows its potential for phase-matched frequency conversion within the transparency range up to 8 μm [17]. Waveguides were demonstrated in $Sn_2P_2S_6$ by He^+ implantation [18] and $Sn_2P_2S_6$ nanoparticles are used for enhancing the electro-optic effect of liquid crystals [19].

$Sn_2P_2S_6$ crystals are grown by the conventional chemical vapor-transport growth technique [20] using iodine (I) as a transport agent. This can be loaded in the tube in pure state or in composition with tin (Sn). SnI_4 is typically used to grow nominally pure $Sn_2P_2S_6$ crystals of yel-

low color, which show a two-wave mixing gain Γ of $\sim$2.5 cm^{-1} at 780 nm [14]. By increasing the temperature gradient during growth and using SnI_2 as the transport agent, modified $Sn_2P_2S_6$ crystals of brown color were obtained. These have presumably a variation of nonstoichiometric defects, i.e., an increased concentration of sulfur vacancies [21] and show a very large two-wave mixing gain Γ of 18 cm^{-1} at 780 nm [14].

A more common and controllable approach to improve the sensitivity of photorefractive crystals is doping. In this work, we report on the photorefractive properties of new $Sn_2P_2S_6$ crystals doped with tellurium (Te) or antimony (Sb). Te and Sb are chosen as dopants, because they are in the same group in the periodic system as sulfur (S) and phosphor (P), respectively, and are therefore potential substitutes in the crystal lattice of $Sn_2P_2S_6$ for S and P. Doping is obtained by adding the doping material into the initial compound in the chemical vapor-transport growth. Te-doped $Sn_2P_2S_6$ ($Sn_2P_2S_6$:Te) was already successfully implemented in optical phase conjugation at 1064 nm [15]. However, important photorefractive parameters were not reported yet for this material, except for preliminary results at the wavelength of 780 nm [22]. Here we investigate both $Sn_2P_2S_6$:Te and $Sn_2P_2S_6$:Sb to determine the most important photorefractive parameters for applications in the red and infrared from 633 to 1064 nm. We measure the two-wave mixing gain Γ and the two-wave mixing response time τ, and determine photorefractive parameters such as the effective electro-optic coefficient r_{eff}, the effective number of traps N_{eff}, and the diffusion length L_D. The results are compared with conventional yellow $Sn_2P_2S_6$ and modified brown $Sn_2P_2S_6$.

2. EXPERIMENT

A. Crystals

The $Sn_2P_2S_6$ crystals used in our experiments were grown by the conventional chemical vapor-transport growth technique with the dopant material in the initial compound. Crystals doped with Te are of light brown color and crystals doped with Sb are of light red color. In the following, we are investigating Te-doped crystals with an amount of 1%, 1.5%, 2%, and 3% of Te in the initial compound and one crystal with 1% Sb.

At room temperature, $Sn_2P_2S_6$ has a ferroelectric monoclinic structure with point group m [10]. We use a coordinate system with the z axis parallel to the crystallographic c axis, the y axis normal to the mirror plane, and the x axis (that is close to the axis of spontaneous polarization) normal to y and z [10]. The samples were oriented by x rays, cut along the x, y, and z axes and polished normal to the z axis. Crystals were poled by applying an electric field of $\sim$500 V/cm normal to the x faces above the phase transition temperature T_c=337 K and then slowly cooled down to room temperature with the applied electric field.

Optical absorption coefficients were obtained by transmission measurements with a Perkin Elmer λ9 spectrophotometer. Spectra were measured with light polarized along the x axis and analyzed taking into account multiple reflections at the surfaces on the base of the refractive index dispersion data [23]. The crystals we used had

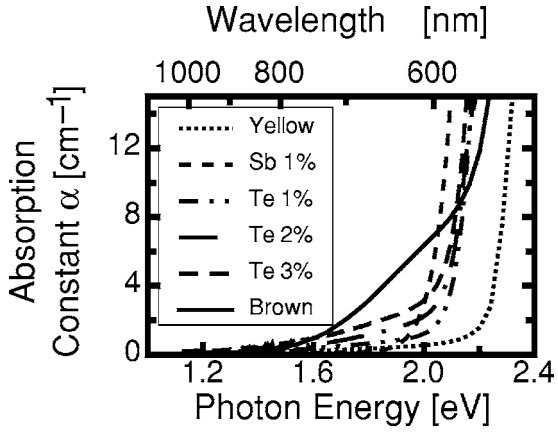

Fig. 1. Absorption spectra of nominally pure yellow, brown, Sb- and Te-doped $Sn_2P_2S_6$ crystals for x-polarized light.

the following thicknesses: 0.2 cm for $Sn_2P_2S_6$:Te 1%, 0.22 cm for $Sn_2P_2S_6$:Te 1.5%, 0.38 cm for $Sn_2P_2S_6$:Te 2%, 0.33 cm for $Sn_2P_2S_6$:Te 3%, and 0.24 cm for $Sn_2P_2S_6$:Sb 1%. Figure 1 shows the absorption coefficients as a function of the photon energy $h\nu$ (wavelength λ) for Te- and Sb-doped $Sn_2P_2S_6$. For comparison, we also show data for undoped crystals, i.e., brown and yellow $Sn_2P_2S_6$, that were obtained in [14]. One can see that the brown crystal reveals an enhanced absorption band leading to a significant rise of the absorption coefficient in the red. The absorption spectra of Te-doped crystals also show an additional absorption band that increases with Te concentration. Additionally, the edge of transparency ($\sim$15 cm^{-1}) for all three doping levels is shifted by $\sim$0.2 eV toward longer wavelengths. For the Sb-doped crystal, the absorption edge is also shifted to a higher wavelength compared with pure $Sn_2P_2S_6$, by $\sim$0.3 eV, and the absorption band in the red is less pronounced, with a steep drop of the absorption for decreasing photon energy below the bandgap. The absorption values in the infrared remain low ($<$0.1 cm^{-1}) in all investigated samples.

B. Photorefractive Measurements

To determine the two most important photorefractive parameters for applications (the two-wave mixing gain Γ and a response time constant τ), we performed two-wave mixing measurements for all the samples at different wavelengths using the usual experimental setup [1]. As light sources we used a HeNe laser for 633 nm (maximal output power P_{max}=5 mW), single-mode laser diodes for 780 nm (P_{max}=100 mW, Rainbow Photonics), and for 980 nm (P_{max}=100 mW, Semiconductor Laser International), a Ti:sapphire laser for 860 nm (P_{max}=100 mW, Coherent) and a Nd:YAG laser for 1064 nm (P_{max} =400 mW, Lightwave Electronics). The beam was extraordinarily polarized and divided into two beams by a beam splitter. A neutral density filter reduced the intensity of the signal beam to have a high-intensity ratio of the pump to signal beam to ensure negligible depletion of the pump beam. The two beams were overlapping with an external angle of 2θ. The bisector of the two beams was directed along the z axis of the crystal, and both beams propagated in the xz plane. By varying the angle 2θ, the two-wave mixing experiment can be carried out at differ-

ent grating spacings $\theta = \lambda/(2\sin\theta)$, where λ is the light wavelength in vacuum. For all the samples and wavelengths, the amplification was in the direction of the $+x$-crystalline axis, implying that holes are the dominant charge carriers.

For the diffusion case, one can express the stationary two-beam coupling gain coefficient within the weak probe beam approximation as a function of the grating spacing [24]:

$$\Gamma = \frac{4\pi^2 k_B T}{\lambda e} n_S n_P^2 \frac{\cos 2\Theta_S}{\cos \Theta_S} r_{\text{eff}} \frac{1}{\Lambda\left[1 + \left(\frac{2\pi l_s}{\Lambda}\right)^2\right]}, \qquad (1)$$

where k_B is the Boltzmann constant, T is the absolute temperature, e is the unit charge, n_S and n_P are refractive indices of the signal and the pump beams, Θ_S is the internal angle between the signal beam and the sample normal, r_{eff} is the effective electro-optic coefficient, and $l_s = \sqrt{\epsilon_{\text{eff}}\epsilon_0 k_B T/(e^2 N_{\text{eff}})}$ is the Debye screening length. Here ϵ_0 is the electric constant, ϵ_{eff} is the effective dielectric constant, and N_{eff} is the effective concentration (number per unit volume) of traps. In Eq. (1), effects of beam walk-off and of a possible anisotropy of the photoexcitation cross section were neglected [25].

Figure 2 shows the measured dependence of the steady-state two-wave mixing gain Γ on the grating spacing Λ for the $Sn_2P_2S_6$:Te 1.5% crystal. Measurements at the wavelengths 633, 860, and 1064 nm are presented. For these wavelengths the maximal two-wave mixing gain coefficients are 17, 8, and 4.5 cm^{-1}, respectively. The solid curves correspond to the theoretical dependence according to Eq. (1). For the evaluation, we use the effective dielectric constant $\epsilon_{\text{eff}} \approx 280$ [22] and the refractive indices $n_S = n_P \approx 3.06$ at 633 nm, 2.90 at 860 nm, and 2.84 at 1064 nm [23]. From the model parameters, we can estimate the effective electro-optic coefficient r_{eff} and the effective concentration of traps N_{eff}. The parameters derived from Eq. (1) are listed in Table 1. Two-wave mixing measurements for the crystals $Sn_2P_2S_6$:Te 1.0%, $Sn_2P_2S_6$:Te 2.0%, $Sn_2P_2S_6$:Te 3.0%, and $Sn_2P_2S_6$:Sb 1.0% have also been performed at the wavelengths in the infrared mentioned before. The parameters derived from these measurements are listed in Table 1. The dielectric constant $\epsilon_{11} = 280 \pm 50$ of Sb-doped $Sn_2P_2S_6$ was measured and is similar to the one determined in Te-doped samples. For comparison, the values for pure (yellow) $Sn_2P_2S_6$ and modified (brown) $Sn_2P_2S_6$ are included in Table 1 as well.

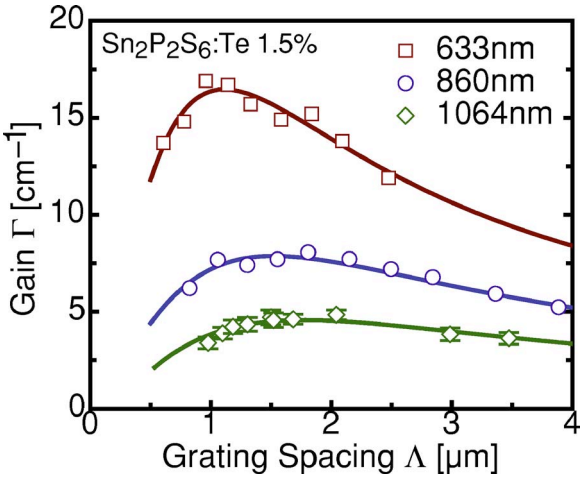

Fig. 2. (Color online) Two-wave mixing gain Γ as a function of the grating spacing Λ in 1.5% Te-doped $Sn_2P_2S_6$ for x-polarized light for the wavelengths 633, 860, and 1064 nm. Solid curves are theoretical curves according to Eq. (1) and parameters listed in Table 1.

The build-up time of the two-wave mixing gain Γ after switching on the writing beams in the two-wave mixing experiment can be described in the simplest approximation with a single exponential function and one time constant τ:

$$\Gamma = \Gamma_0(1 - e^{-t/\tau}). \qquad (2)$$

In Eq. (2) Γ_0 is the saturation value. In some two-wave mixing measurements, depending on the wavelength and grating spacing, we observe that the dynamics cannot be described by a single exponential function. A typical measurement for such a temporal evolution of the two-wave mixing gain Γ is shown in Fig. 3. We therefore use a double-exponential dynamics,

$$\Gamma = \Gamma_1(1 - e^{-t/\tau_1}) + \Gamma_2(1 - e^{-t/\tau_2}). \qquad (3)$$

This dynamics with a "fast" (τ_1) and a "slow" (τ_2) component can be explained by the presence of multiple energy levels inside the energy bandgap [10]. The second contribution (Γ_2) was of the same sign as Γ_1, and therefore it is not caused by electron-hole compensation as observed in nominally pure yellow samples of type I [10,13]. The two-wave mixing gain Γ_1 (the fast component) is ~1 order of magnitude larger than Γ_2. Therefore in the following we only consider the fast two-wave mixing rise time τ_1 as the rise time and neglect the slow contribution.

The response time τ for negligible dark conductivity is given by [23]

$$\tau = \tau_{\text{die}} \frac{1 + (2\pi L_D/\Lambda)^2}{1 + (l_s/\Lambda)^2}, \qquad (4)$$

where $\tau_{\text{die}} = \epsilon_0\epsilon_{\text{eff}}/\sigma$ is the dielectric relaxation time and $\sigma = e\mu n_0$ the photoconductivity, where n_0 is the steady-state concentration of free charge carriers and is proportional to the total light intensity I_0. $L_D = \sqrt{k_B T\mu/(e\gamma N_A)}$ is the diffusion length, where γ is the recombination constant, μ is the carrier mobility, and N_A is the concentration of traps in the dark.

Figure 4 shows the measured two-wave mixing build-up time as a function of the grating spacing Λ for $Sn_2P_2S_6$:Te 1.5%. Measurements for the infrared wavelengths 980 and 1064 nm are presented. The measurements were done at intensities 6.4 and 6.2 W/cm^2 for 980 and 1064 nm, respectively. For comparing the measurements at different wavelengths, the data points in Fig. 4 were normalized to an intensity of 10 W/cm^2, based on the measured linear dependence of the build-up rate with intensity. Additionally, the wavelength-dependent Fresnel losses at the $Sn_2P_2S_6$ surface have been considered also. The solid curves correspond to the theoretical dependence given by Eq. (4) with parameters that correspond best to the measurements, considering the Debye screening length l_S as obtained from the $\Gamma(\Lambda)$ measurements. From

Table 1. Photorefractive Parameters of Te- and Sb-Doped $Sn_2P_2S_6$[a] Compared with Nominally Pure $Sn_2P_2S_6$ and Modified Brown $Sn_2P_2S_6$[b]

$Sn_2P_2S_6$ Sample	λ (nm)	α_x (cm^{-1})	Γ_{max} (cm^{-1}) (±10%)	L_D (μm) (±50%)	r_{eff} (pm/V) (±15%)	τ_{die} at 10 W/cm^2 (ms) (±20%)	$\tau(\Gamma_{max})$ at 10 W/cm^2 (ms) (±20%)	N_{eff} (10^{16} cm^{-3}) (±15%)
Nominally pure	633	0.5	4–7	0.2			1–5	0.7
(type II) yellow	780	0.20	2.5		41		10	0.2
	860	0.16	1.8	0.9	48	9	12	0.08
	980	0.12	1.6	1.4	40	15	44	0.11
	1064	0.10	0.9		38			0.044
Brown	633	5.7	38	0.1		0.2	0.4	2.5
	780	0.9	18		180	0.4	1	0.7
	860	0.3	14		190			0.48
	980	0.14	11	0.5	190	29	33	0.39
	1064	**0.09**	**8.6**		160			0.04
SPS:Te 1.0%	633	1.0	10	0.5	60	0.1	0.3	0.9
	780	0.34	6	2.3	50	0.2	1.3	1.0
	860	0.19	6.5	0.5	89	6	10	0.44
	980	0.11	6	0.3	75	8	13	0.62
	1064	0.09	4.5					
SPS:Te 1.5%	860	0.8	8	0.5	89	7	15	0.44
	980	0.42	6	0.5	83	10	13	0.57
	1064	**0.36**	**4.5**	0.6	73	**11**	25	0.53
SPS:Te 2.0%	633	1.8	10	1.1	57	0.2	0.5	1.0
	780	0.6	6	0.8	47	0.5	1.6	0.8
	1064	0.10	2.2	0.9	54	17	32	0.22
SPS:Te 3.0%	633	2.7	12	2.6	81	0.1	0.4	0.8
	780	0.9	7	0.7	56	0.6	1.3	0.8
	1064	0.20	2.5	0.8	49	14	20	0.34
SPS:Sb 1.0%	633	1.4	20	0.7	110	0.2	0.4	1.0
	780	0.08	0.4					

[a]This work.

[b]This work and [14,26].

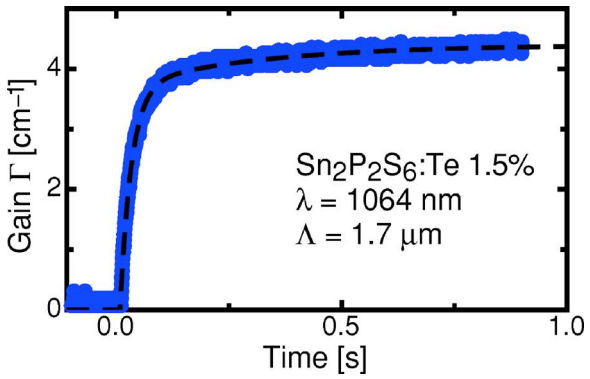

Fig. 3. (Color online) Temporal evolution of the two-wave mixing gain Γ after turning on the pump beam at time $t=0$, in a 1.5% Te-doped $Sn_2P_2S_6$ crystal at a wavelength of 1064 nm, light intensity of 6 W/cm^2, and a grating spacing $\Lambda=1.7$ μm. The dashed curve is theoretical according to Eq. (3) with a "fast" time constant $\tau_1=25$ ms and a "slow" time constant $\tau_2=310$ ms.

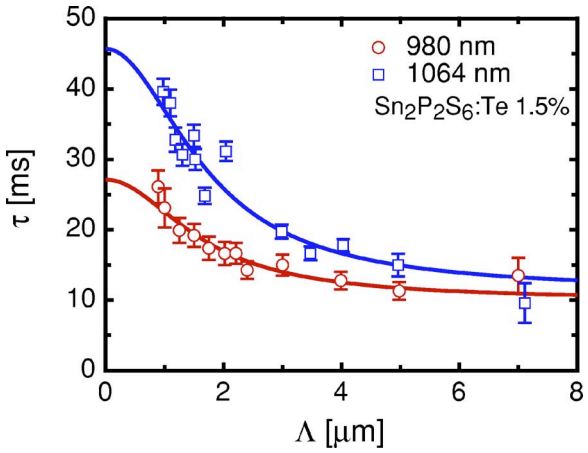

Fig. 4. (Color online) Two-wave mixing response time τ as a function of the grating spacing Λ in 1.5% Te-doped $Sn_2P_2S_6$ for the wavelengths 980 and 1064 nm, normalized to an intensity of 10 W/cm^2.

Eq. (4), we can estimate the diffusion length L_D and the dielectric relaxation time τ_{die}. The obtained parameters for this crystal and for other $Sn_2P_2S_6$ crystals are listed in Table 1. The value of L_D is basically determined by two-wave mixing rise times for small grating spacings. Therefore the error for L_D can be as high as ±50%. In Table 1, the response times τ_{die} and the rise time at the grating spacing with maximal two-wave mixing gain $\tau(\Gamma_{max})$ have also been normalized to an intensity of 10 W/cm^2, assuming a linear dependence τ^{-1} on I_0.

3. DISCUSSION

In Section 2, we have seen that the measured rise time to build up a photorefractive grating is the fastest in Te-doped $Sn_2P_2S_6$ among the different $Sn_2P_2S_6$ crystals. Since this rise time is very fast as compared with other ferroelectrics (e.g., 2 orders of magnitude faster than in Rh-doped $BaTiO_3$), it is of interest to compare it with the fundamental limit for the speed of the photorefractive effect. For this purpose, we estimate a lower limit for the rise time to build up the refractive index grating in the crystal. Assuming that the separation of a pair of charge carriers needs at least one photon, we can calculate the necessary energy to build a volume index grating consisting of N separated charge carriers in the crystal. Out of the incoming beam with an intensity I_0, only a part of it is absorbed in the crystal, as determined by the absorption coefficient α. Additionally, only a part of the absorbed beam will excite charges that will build a grating, described by the quantum efficiency for the photoexcitation η. The minimum rise time, i.e., the time needed to excite the amount of charges needed to build up the steady-state grating, can be approximated by [27],

$$t_{\min} = \left(\frac{h\nu}{e}\right)\left(\frac{\lambda}{\Lambda}\right)\left(\frac{\Gamma}{\alpha}\right)\frac{2}{\pi\eta I_0 n^3 r_{\text{eff}}}\frac{\epsilon_0\epsilon}{}, \tag{5}$$

where e is the electron charge.

As examples, we calculate the minimal photorefractive rise time for the $Sn_2P_2S_6$:Te 1.0% crystal at the wavelength of 633 nm and for the $Sn_2P_2S_6$:Te 1.5% crystal at 1064 nm. Considering an ideal photoexcitation efficiency $\eta=1$ and a grating spacing Λ at the maximum gain Γ, i.e., $\Lambda=1.0$ μm for 633 nm and $\Lambda=1.5$ μm for 1064 nm. We get $t_{\min}\approx 0.1\pm 0.02$ ms, which is only approximately three times faster, and $t_{\min}\approx 0.2\pm 0.1$ ms, which is $\sim$120 times faster compared with the experimentally measured buildup that also includes the redistribution of the charge carriers. The larger error for the rise time $t_{\min}$ at 1064 nm is due to the larger error of the measured absorption constant at 1064 nm. This means that at 633 nm we are closer to the fundamental limit than at 1064 nm. We attribute this difference to different values of the quantum efficiency η at different wavelengths, i.e., photoexcited charge carriers at 633 nm contribute more efficiently to the photorefractive grating than at 1064 nm.

In the model we used for describing the photorefractive effect in $Sn_2P_2S_6$, we assumed one energy level in the bandgap [24]. This model predicts the following relationship for the response rate: $1/\tau_{\text{die}}\sim I_0\alpha$ for the same crystal at different wavelengths. This correlation is not fulfilled in our $Sn_2P_2S_6$ crystals (see Table 1), although we observed a linear increase of the response rate as a function of intensity I_0 at certain wavelengths. This shows that the theoretical model with one energy level is not sufficient to describe the wavelength dependence, and that in the photorefractive response in $Sn_2P_2S_6$ several energy levels are involved.

The diffusion length L_D was determined with a big error, therefore a comparison cannot be made; however, it has a similar order of magnitude in all the samples and is smaller than the Debye grating spacing $\Lambda_{\max}=\sqrt{\epsilon_0\epsilon_{\text{eff}}k_BT/(e^2N_{\text{eff}})}$ where the maximum two-wave mixing gain $\Gamma_{\max}$ is obtained. According to the coupled-wave theory [24] this implies that $\tau_{\text{die}}<\tau_{\Gamma_{\max}}$ in all the samples.

Compared with pure yellow $Sn_2P_2S_6$ in all Te-doped $Sn_2P_2S_6$ crystals, an increase of the effective trap concentration N_{eff} has been measured (determined) in the considered wavelength range. While at 633 nm, the values for doped and pure yellow samples do not differ considerably, the difference is larger going to higher wavelengths, e.g., 1 order of magnitude for $Sn_2P_2S_6$:Te 1.5% at 1064 nm. We get the highest values for N_{eff} in the $Sn_2P_2S_6$:Te 1.5% sample, i.e., an additional amount of Te in the initial compound does not lead to an increased effective concentration of traps N_{eff}. The wavelength dependence of N_{eff} can also be attributed to multiple energy levels involved in the photorefractive response of $Sn_2P_2S_6$, as also observed in other materials, e.g., in CdTe [28] and Rh:$BaTiO_3$ [29]. This dependence is especially strong in nominally pure (yellow), modified (brown), and Sb-doped crystals, while in Te-doped samples N_{eff} decreases much less with increasing wavelength. Therefore the photorefractive centers in Te-doped samples may have a different origin as in nominally pure and modified samples.

In photorefractive measurements, one often has to consider an effective electro-optic coefficient $r_{\text{eff}}=r'_{\text{eff}}\xi$, where r'_{eff} is a combination of the strain-free electro-optic contribution and the elasto-optic contribution [25]. ξ is a reduction factor, which lowers the apparent effective electro-optic coefficient r'_{eff} in photorefractive measurements, due to, e.g., electron-hole competition. From direct interferometric measurements, the electro-optic coefficients were determined, e.g., $r_{111}=174\pm 10$ pm/V at 633 nm, with a low dispersion in the near infrared [12]. For pure yellow $Sn_2P_2S_6$, we get the lowest values for r_{eff} and for brown $Sn_2P_2S_6$, r_{eff} is not reduced, i.e., within the error we get the same values as in the direct interferometric measurements. In Te-doped $Sn_2P_2S_6$ crystals, the 1.5% sample has the highest values for r_{eff}.

Figure 5 shows the maximal two-wave mixing gain $\Gamma_{\max}$ as a function of the photon energy $h\nu$. Measurements for yellow, brown, Sb-doped, and 1% Te-doped $Sn_2P_2S_6$ are presented. Doping of $Sn_2P_2S_6$ with more than 1.5% Te

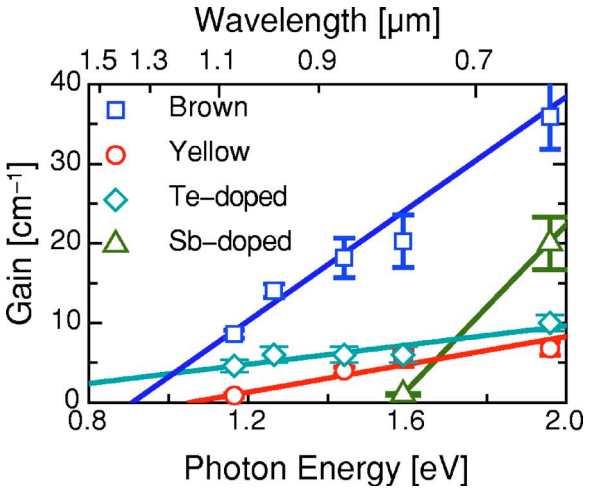

Fig. 5. (Color online) Measured maximal two-wave mixing gain coefficient as a function of the photon energy $h\nu$. Solid lines are guides for the eyes.

in the starting material increases the absorption (Fig. 1) but does not lead to an improvement of the photorefractive properties (see Table 1). The solid lines in Fig. 5 are guides for the eyes and were calculated with the linear function $\Gamma(h\nu)$ with a remarkably different slope for each $Sn_2P_2S_6$ material. Brown and Sb-doped $Sn_2P_2S_6$ have a slope of more than five times higher compared with yellow and Te-doped $Sn_2P_2S_6$. Therefore, although the maximal two-wave mixing gain $\Gamma_{max} = 10\ cm^{-1}$ of $Sn_2P_2S_6$:Te 1% at 633 nm is only about half as high as that of $Sn_2P_2S_6$:Sb, it is still $\sim 4.5\ cm^{-1}$ at 1064 nm; whereas in Sb-doped crystals, we see practically no photorefractive response already at 780 nm. Although the defect centers that are responsible for photorefraction in $Sn_2P_2S_6$ are not yet clearly identified, we can conclude that several different energy levels are involved in the photorefractive response of $Sn_2P_2S_6$, and their contribution can be altered considerably by doping. Te doping is best to increase the photorefractive sensitivity in the infrared and is therefore the most attractive for wavefront corrections and improvements of the spectral properties of infrared laser sources. On the other hand, Sb doping can be used to effectively suppress the photorefraction in the infrared, which is desired, e.g., for electro-optic and nonlinear optical applications.

4. CONCLUSION

In summary, $Sn_2P_2S_6$ can be efficiently modified by doping with Te and Sb. Two-wave mixing measurements show an increased two-wave mixing gain at 633 nm for Te- and Sb-doped $Sn_2P_2S_6$ (10 and 20 cm^{-1}, respectively) compared with nominally pure conventional yellow $Sn_2P_2S_6$ (4–7 cm^{-1}). Te-doped $Sn_2P_2S_6$ shows a favorable photorefractive sensitivity for higher wavelengths in the infrared, e.g., a two-wave mixing gain $4.5\ cm^{-1}$ at 1064 nm. Sb doping, on the other hand, suppresses the photorefraction in the near infrared and shows practically no response already at 780 nm. Compared with modified brown $Sn_2P_2S_6$, the two-wave mixing gain for Te-doped $Sn_2P_2S_6$ is lower in the measured wavelength range of 633–1064 nm. However, in the investigated wavelength range, the photorefractive gain of brown crystals decreases much more rapidly when increasing the wavelength, while for Te-doped crystals, we can expect a substantial response in the infrared also beyond the investigated range. Additionally, due to the better growth control of Te-doped $Sn_2P_2S_6$ and the possibility to grow crystals of more than 1 cm in length L, the important parameter, coupling strength ΓL for applications is the highest in Te-doped $Sn_2P_2S_6$. The photorefractive response is fast for all measured modified $Sn_2P_2S_6$ crystals, e.g., Te-doped $Sn_2P_2S_6$ with a two-wave mixing rise time of $\sim$20 ms at a wavelength of 1064 nm for an intensity of $6\ W/cm^2$. Therefore Te-doped $Sn_2P_2S_6$ can be considered as presently the best photorefractive material in the near infrared up to a wavelength of 1.06 μm.

ACKNOWLEDGMENTS

We are grateful to Ivan M. Stoika for the crystal growth and to Jaroslav Hajfler for crystal preparation. The research has been supported by the Swiss National Foundation.

REFERENCES

1. P. Günter and J.-P. Huignard, eds., *Photorefractive Materials and Their Applications I* (Springer-Verlag, 2006).
2. B. A. Wechsler, M. B. Klein, C. C. Nelson, and R. N. Schwartz, "Spectroscopic and photorefractive properties of infrared-sensitive rhodium-doped barium titanate," Opt. Lett. **19**, 536–538 (1994).
3. M. Ewart, R. Ryf, C. Medrano, H. Wüest, M. Zgonik, and P. Günter, "High photorefractive sensitivity at 860 nm in reduced rhodium-doped $KNbO_3$," Opt. Lett. **22**, 781–783 (1997).
4. A. Brignon, J. P. Huignard, M. H. Garrett, and I. Mnushkina, "Spatial beam cleanup of a Nd:YAG laser operating at 1.06 μm with two-wave mixing in Rh:$BaTiO_3$," Appl. Opt. **36**, 7788–7793 (1997).
5. L. Lombard, A. Brignon, J. P. Huignard, E. Lallier, G. Lucas-Leclin, P. Georges, G. Pauliat, and G. Roosen, "Diffraction-limited polarized emission from a multimode ytterbium amplifier after a nonlinear beam converter," Opt. Lett. **29**, 989–991 (2004).
6. S. MacCormack and J. Feinberg, "High-brightness output from a laser-diode array coupled to a phase-conjugating mirror," Opt. Lett. **18**, 211–213 (1993).
7. P. D. van Voorst, H. L. Offerhaus, and K. J. Boller, "Single-frequency operation of a broad-area laser diode by injection locking of a complex spatial mode via a double phase conjugate mirror," Opt. Lett. **31**, 1061–1063 (2006).
8. G. Roosen, A. Godard, S. Maerten, V. Reboud, N. Dubreuil, and G. Pauliat, "Self-organization of laser cavities using dynamic holograms," Opt. Mater. **23**, 289–293 (2003).
9. G. Roosen, S. Bernhardt, and P. Delaye, "$Ba_{0.77}Ca_{0.23}TiO_3$: a new photorefractive material to replace $BaTiO_3$ in applications," Opt. Mater. **23**, 243–251 (2003).
10. A. A. Grabar, M. Jazbinsek, A. N. Shumelyuk, Yu. M. Vysochanskii, G. Montemezzani, and P. Günter, "Photorefractive effects in $Sn_2P_2S_6$," in *Photorefractive Materials and Their Applications II*, P. Günter and J.-P. Hiugnard, eds. (Springer-Verlag, 2007).
11. S. G. Odoulov, A. N. Shumelyuk, U. Hellwig, R. A. Rupp, and A. A. Grabar, "Photorefractive beam coupling in tin hypothiodiphosphate in the near infrared," Opt. Lett. **21**, 752–754 (1996).
12. D. Haertle, G. Caimi, A. Haldi, G. Montemezzani, P. Günter, A. A. Grabar, I. M. Stoika, and Yu. M. Vysochanskii, "Electro-optical properties of $Sn_2P_2S_6$," Opt. Commun. **215**, 333–343 (2003).
13. A. N. Shumelyuk, A. Hryhorashchuk, and S. G. Odoulov, "Coherent optical oscillator with periodic zero-π phase modulation," Phys. Rev. A **72**, 023819 (2005).
14. M. Jazbinsek, D. Haertle, G. Montemezzani, P. Günter, A. A. Grabar, I. M. Stoika, and Y. M. Vysochanskii, "Wavelength dependence of visible and near-infrared photorefraction and phase conjugation in $Sn_2P_2S_6$," J. Opt. Soc. Am. B **22**, 2459–2467 (2005).
15. T. Bach, M. Jazbinsek, P. Günter, A. A. Grabar, I. M. Stoika, and Y. M. Vysochanskii, "Self pumped optical phase conjugation at 1.06 μm in Te-doped $Sn_2P_2S_6$," Opt. Express **13**, 9890–9896 (2005).
16. R. Mosimann, D. Haertle, M. Jazbinsek, G. Montemezzani, and P. Günter, "Interband photorefraction in $Sn_2P_2S_6$ at visible wavelengths," J. Opt. Soc. Am. B **23**, 1620–1625 (2006).
17. D. Haertle, M. Jazbinsek, G. Montemezzani, and P. Günter, "Nonlinear optical coefficients and phase-matching conditions in $Sn_2P_2S_6$," Opt. Express **13**, 3765–3776 (2005).
18. A. Guarino, M. Jazbinsek, C. Herzog, R. Degl'Innocenti, G. Poberaj, and P. Günter, "Optical waveguides in $Sn_2P_2S_6$ by low fluence MeV He^+ ion implantation," Opt. Express **14**, 2344–2358 (2006).
19. O. Buchnev, A. Glushchenko, Y. Reznikov, V. Reshetnyak, O. Tereshchenko, and J. West, "Diluted ferroelectric suspension of $Sn_2P_2S_6$ nanoparticles in nematic liquid crystals," Proc. SPIE **5257**, 7–12 (2003).
20. C. D. Carpentier and R. Nitsche, "Vapor growth and crystal

data of thio(seleno)-hypodiphosphates $Sn_2P_2S_6$, $Sn_2P_2Se_6$, $Pb_2P_2S_6$, $Pb_2P_2Se_6$ and their mixed-crystals," Mater. Res. Bull. **9**, 401–410 (1974).
21. Z. Potucek and Z. Bryknar, "Photoluminescence of defects in $Sn_2P_2S_6$ crystals," Ferroelectrics **334**, 171–179 (2006).
22. A. A. Grabar, I. V. Kedyk, I. M. Stoika, Yu. M. Vysochanskii, M. Jazbinsek, G. Montemezzani, and P. Günter, Enhanced photorefractive properties of Te-Doped $Sn_2P_2S_6$, in *Photorefractive Effects, Materials, and Devices*, Vol. 87 of OSA Trends in Optics and Photonics Series (Optical Society of America, 2003), pp. 10–14.
23. D. Haertle, A. Guarino, J. Hajfler, G. Montemezzani, and P. Günter, "Refractive indices of $Sn_2P_2S_6$, at visible and infrared wavelengths," Opt. Express **13**, 2047–2057 (2005).
24. N. V. Kukhtarev, V. B. Markov, S. G. Odoulov, M. S. Soskin, and V. L. Vinetskii, "Holographic storage in electrooptic crystals 2. Beam coupling—light amplification," Ferroelectrics **22**, 961–964 (1979).
25. G. Montemezzani and M. Zgonik, "Space-charge driven holograms in anisotropic media," in *Photorefractive Materials and Their Applications I*, P. Günter and J.-P. Hiugnard, eds. (Springer-Verlag, 2006).
26. A. A. Grabar, I. V. Kedyk, M. I. Gurzan, I. M. Stoika, A. A. Molnar, and Yu. M. Vysochanskii, "Enhanced photorefractive properties of modified $Sn_2P_2S_6$," Opt. Commun. **188**, 187–194 (2001).
27. P. Yeh, "Fundamental limit of the speed of photorefractive effect and its impact on device applications and material research," Appl. Opt. **26**, 602–605 (1987).
28. Ph. Delaye, L. A. de Montmorillon, I. Baggio, J. C. Launay, and G. Roosen, "Wavelength dependent effective trap density in CdTe: evidence for the presence of two photorefractive species," Opt. Commun. **134**, 580–590 (1997).
29. M. Chi, S. X. Dou, Y. Zhu, and P. Ye, "Wavelength dependence of the effective trap density in Rh-doped $BaTiO_3$: a comparison between theory and experiment," Opt. Commun. **170**, 115–120 (1999).